Modeling DNA trapping of anticancer therapeutic targets using missense mutations identifies dominant synthetic lethal interactions

Akil Hamza[a,1], Leanne Amitzi[a,1], Lina Ma[a], Maureen R. M. Driessen[a], Nigel J. O'Neil[a], and Philip Hieter[a,2]

[a]Michael Smith Laboratories, University of British Columbia, Vancouver, BC V6T 1Z4, Canada

Contributed by Philip Hieter, February 26, 2021 (sent for review January 7, 2021; reviewed by Jasper Rine and Mike Tyers)

Genetic screens can identify synthetic lethal (SL) interactions and uncover potential anticancer therapeutic targets. However, most SL screens have utilized knockout or knockdown approaches that do not accurately mimic chemical inhibition of a target protein. Here, we test whether missense mutations can be utilized as a model for a type of protein inhibition that creates a dominant gain-of-function cytotoxicity. We expressed missense mutations in the *FEN1* endonuclease and the replication-associated helicase, *CHL1*, that inhibited enzymatic activity but retained substrate binding, and found that these mutations elicited a dominant SL phenotype consistent with the generation of cytotoxic protein–DNA or protein–protein intermediates. Genetic screens with nuclease-defective h*FEN1* and helicase-deficient y*CHL1* captured dominant SL interactions, in which ectopic expression of the mutant form, in the presence of the wild-type form, caused SL in specific mutant backgrounds. Expression of nuclease-defective h*FEN1* in yeast elicited DNA binding-dependent dominant SL with homologous recombination mutants. In contrast, dominant SL interactions with helicase-deficient y*CHL1* were observed in spindle-associated, Ctf18-alternative replication factor C (Ctf18-RFC) clamp loader complex, and cohesin mutant backgrounds. These results highlight the different mechanisms underlying SL interactions that occur in the presence of an inhibited form of the target protein and point to the utility of modeling trapping mutations in pursuit of more clinically relevant SL interactions.

dominant synthetic lethality | Fen1 endonuclease | Chl1 helicase | DNA trapping | dominant missense mutations

Tumor-specific genetic alterations represent vulnerabilities that can be leveraged to selectively target tumors with therapeutics (1). This can be achieved by exploiting the concept of synthetic lethality (SL), which occurs when cells carrying perturbations of two genes individually are viable but combining those perturbations results in cell lethality (2). However, while the concept of SL holds great promise, and many cancer-relevant SL genetic interactions have been identified over the past two decades, only one SL-based therapeutic has reached the clinic (3).

A number of factors confound the development of SL-based therapies, such as the context dependency of genetic interactions and the complexity of overlapping functions between different complexes and pathways in the DNA damage response (3). The success rate of SL-based therapeutics could conceivably be improved by analyzing the properties of PARP inhibitors, which are the only SL-based therapeutic currently in the clinic. Inhibitors of the proteins PARP-1 and PARP-2, which are implicated in DNA repair and genome maintenance (4), were specifically developed as SL-based therapeutics for the treatment of homologous recombination (HR) repair-deficient tumors (5–7). Research into the mechanism of PARP SL has found that the cytotoxicity of PARP inhibitors derives not from the loss of PARP activity, per se, but rather from the trapping of PARP protein on DNA generating a PARP–DNA cytotoxic lesion. The trapped protein–DNA lesion not only generates a potentially cytotoxic lesion, it may also prevent other repair proteins from accessing the DNA damage. The PARP-DNA lesion requires BRCA-mediated HR for error-free resolution or bypass during replication. Consistent with this model, PARP inhibitors are more effective at killing *BRCA*-mutated cancer cells than *PARP* knockout or knockdown, and the cytotoxicity of PARP inhibitors correlates with their trapping ability (8–10).

Another class of anticancer therapeutic that traps protein targets on DNA is topoisomerase inhibitors. Many topoisomerase inhibitors act as interfacial inhibitors and interfere with the catalytic cycle, preventing the resolution of a DNA–topoisomerase intermediate, thereby creating a trapped topoisomerase–DNA adduct (11). Although they were not developed as SL-based therapeutics, their efficacy is due in part to SL interactions with tumor-specific mutations affecting replication, checkpoints, or repair (12). For both PARP and topoisomerase inhibitors, the cytotoxicity derives from the formation of a toxic intermediate in the form of an inhibited protein complexed with DNA. In effect, the small molecule inhibitors when bound to their targets convert wild-type protein to a cytotoxic form that creates a "gain-of-function" DNA-damaging agent. The creation of cytotoxic protein–DrNA complexes may be generalizable to other DNA-associated proteins, and it is also possible that inhibitors may result in cytotoxic protein–protein intermediates that indirectly impact DNA processes.

Significance

Although inhibitor-mediated trapping of protein on DNA is a viable anticancer therapeutic strategy, there are very few examples of this approach with clinical applications. One limitation to expanding this strategy is the use of gene knockout-based modeling of chemical inhibition. Instead, we propose mimicking the trapping mechanism of DNA-associated cancer targets using dominant missense mutations. These mutations inhibit enzymatic activity without impacting DNA binding and generate cytotoxic lesions in the presence of the wild-type protein. Trapped cytotoxic lesions impact DNA processes and sensitize cells to deficiencies in some DNA-associated pathways. We identified genetic backgrounds that cannot tolerate the dominant mutant proteins and demonstrated a requirement for DNA or protein binding to maintain this cytotoxicity.

Author contributions: A.H., L.A., N.J.O., and P.H. designed research; A.H., L.A., L.M., and M.R.M.D. performed research; A.H., L.A., and L.M. analyzed data; and A.H., L.A., N.J.O., and P.H. wrote the paper.

Reviewers: J.R., University of California, Berkeley; and M.T., University of Montreal.

The authors declare no competing interest.

See online for related content such as Commentaries.

[1]A.H. and L.A. contributed equally to this work.

[2]To whom correspondence may be addressed. Email: hieter@msl.ubc.ca.

This article contains supporting information online at https://www.pnas.org/lookup/suppl/doi:10.1073/pnas.2100240118/-/DCSupplemental.

Published March 29, 2021.

Most SL screens have relied on loss-of-function knockout/mutation collections, or CRISPR-knockout and RNA interference (RNAi)-based libraries that result in loss- or reduction-of-function phenotypes (3). These approaches may often not accurately model SL interactions between cancer mutations and the chemically inhibited forms of SL partner proteins. An alternative to knockout-based SL modeling is to utilize missense mutations that mimic inhibitors. Missense-derived SL genetic interactions may be more clinically relevant than interactions that are based on complete knockouts as they are assessed when the target protein is present, and retains DNA and/or protein interactions, but is inactivated. For example, specific missense mutations in *Saccharomyces cerevisiae* Top1 enhance the stability of the covalent topoisomerase–DNA intermediate and phenocopy the effect of the topoisomerase inhibitor camptothecin (13). These camptothecin mimetic mutations cause a dominant phenotype and have been used to screen for mutations that sensitize cells to topoisomerase trapping (14).

In both DNA- and protein-trapping scenarios, the trapped inactivated protein would be predicted to elicit a dominant phenotype. This may occur when the trapped protein competes with wild-type protein for substrate and blocks the activity of the wild-type protein. In this way, dominant SL interactions can capture genetic interactions that occur in the presence of the wild-type or residual noninhibited protein. Even trapping of a small percentage of a protein target pool could catalyze a SL interaction and may provide a mechanism by which essential proteins could be exploited to elicit SL.

The efficacy of PARP and topoisomerase inhibitors that trap their targets on DNA suggest that other DNA damage response-associated proteins, in particular those associated with the response to replicative stress, would be good targets for inhibition that causes trapping. The DNA flap endonuclease 1 (FEN1) and the helicase DDX11 are critical enzymes that maintain genome stability during replication and are attractive targets for the development of anticancer therapeutics. FEN1 functions in DNA replication and repair and is required for Okazaki fragment maturation. Due to its key role in DNA replication, FEN1 supports rapid proliferation of cancer cells and is overexpressed in many tumor types (15). DDX11 is a member of the iron sulfur DEAD/DEAH helicase family (16). DDX11 is up-regulated in some primary and metastatic melanomas, and suppression of DDX11 in these melanomas curtails proliferation and induces apoptosis (17). SL interaction screens, utilizing knockout mutants of the yeast ortholog *rad27*Δ, have identified FEN1 as a broad-spectrum target for anticancer therapeutic development (18), especially for HR-deficient tumors (19). The knockout mutant of the DDX11 yeast ortholog *chl1*Δ is also SL with cohesin mutations (20), which are a common genetic vulnerability in a broad range of tumors (21, 22).

In proof-of-principle experiments utilizing yeast-based high-throughput genetic approaches, we used missense mutations in FEN1 and the yeast DDX11 ortholog, Chl1, to mimic a specific case of chemical inhibition in which protein activity was inhibited, but substrate binding was unaffected (23). These mutants were screened for dominant SL interactions with a panel of DNA-associated knockout mutants. Expression of these mutant proteins generated nonoverlapping dominant SL genetic interaction networks and were consistent with the formation of cytotoxic lesions that impacted DNA processes.

Results

Generating Dominant SL Interaction Networks. To screen for dominant SL genetic interactions, we utilized synthetic genetic array (SGA) technology to introduce plasmid-borne, wild-type or missense mutated, inducible open reading frames (ORFs) into an arrayed library of yeast deletion strains. The result is an output array of plasmid-bearing haploid single mutants whose relative fitness can be assessed following induction of either wild-type or mutant ORFs by measuring colony size (Fig. 1*A*). We constructed a miniarray comprising 332 yeast deletion mutants that affect various DNA transactions (Datasets S1–S4). The plasmid-borne ORFs were under the transcriptional regulation of a galactose-inducible promoter and included wild-type or dominant mutants of y*RAD27*, h*FEN1*, or y*CHL1* (Fig. 1 *B*–*E*).

Nuclease-Defective hFEN1 Is Dominant SL with HR Mutants. In vitro competition assays identified the conserved D181A in human FEN1 as a nuclease-defective mutation that retains binding to DNA substrates and could block the activity of wild-type hFEN1 (24, 25). The equivalent missense mutation (D179A) in yRad27 abolishes nuclease activity (26). In vivo assays demonstrated that expression of yeast *rad27-D179A* or human *FEN1-D181A* alleles resulted in dominant effects (27, 28).

Induced ectopic expression of wild-type y*RAD27* or the dominant *rad27-D179A* allele caused profound growth defects in yeast (*SI Appendix*, Fig. S1), and these defects were too severe to yield reliable data from yeast genetic screens. Given that hFEN1 can replace yRad27 and complement loss-of-function phenotypes of the yeast deletion mutant (27, 29), we also conducted the screens with wild-type h*FEN1* and the dominant h*FEN1-D181A* allele. Consistent with previous studies, induced ectopic expression of the human ORFs did not impart severe growth defects in wild-type yeast (*SI Appendix*, Fig. S1), and this was shown to be a result of the reduced binding affinity of human protein to yeast PCNA (a yRad27 binding partner) (27, 30). Therefore, we focused on confirming genetic interaction hits that utilized the human proteins as queries (Fig. 1 *B* and *C*).

We did not find any mutants that had reduced fitness upon induced ectopic expression of h*FEN1*, indicating that the 332 yeast deletion strains can tolerate elevated levels of the wild-type human protein (Dataset S1). We identified 22 putative h*FEN1-D181A* dominant SL interactions that displayed >20% growth defects upon induced ectopic expression (Dataset S2). Quantitative growth curve analysis validated 8 of the dominant SL interactions that resulted upon h*FEN1-D181A* expression (Fig. 1*C* and *SI Appendix*, Fig. S2). This included *rad27*Δ, which was shown previously to have growth defects in response to ectopic expression of the nuclease-defective human protein (endogenous yRad27 can minimize negative effects of dominant nuclease-defective hD181A) (27). Notably, the other 7 dominant SL partner genes all function in the HR-repair pathway, including all members of the MRX complex (y*MRE11*, y*RAD50*, y*XRS2*) and y*RAD55*–y*RAD57* complex. To identify potential false-negative hits in our screen, we selected some mutants from the list of 332 yeast deletion strains for growth curve analysis and determined that the null allele of another HR protein, *rad51*Δ, also had fitness defects upon h*FEN1-D181A* expression (Fig. 1*C*, *SI Appendix*, Fig. S2, and Dataset S2).

The nuclease-defective hD181A protein decreased fitness of yeast HR mutants in the presence of the wild-type yRad27 protein. To confirm if other nuclease-defective hFEN1 mutations that also retain DNA binding have a similar effect, we selected the hR100A mutation, which exhibited these properties in in vitro enzymatic/binding assays (31), and directly tested the ability of this mutant protein to decrease fitness of *rad52*Δ upon ectopic expression. Growth spot assays and liquid growth curve validations confirmed that the hR100A protein decreases fitness of *rad52*Δ mutant cells containing either endogenous wild-type yRad27 (Fig. 2*A*) or wild-type hFEN1 (Fig. 2 *B* and *C*). In contrast, mutations in hFEN1 that have been shown to reduce or abolish binding to DNA substrates in in vitro assays (31) did not impact fitness of *rad52*Δ mutant cells (see Fig. 4). The dominant genetic interactions with h*FEN1-D181A* and h*FEN1-R100A* were stronger in the humanized *rad27*Δ::h*FEN1* yeast strain (*SI Appendix*, Fig. S3), presumably a consequence of the wild-type yeast protein having a stronger competitive effect for yeast DNA substrates than the wild-type hFEN1 protein.

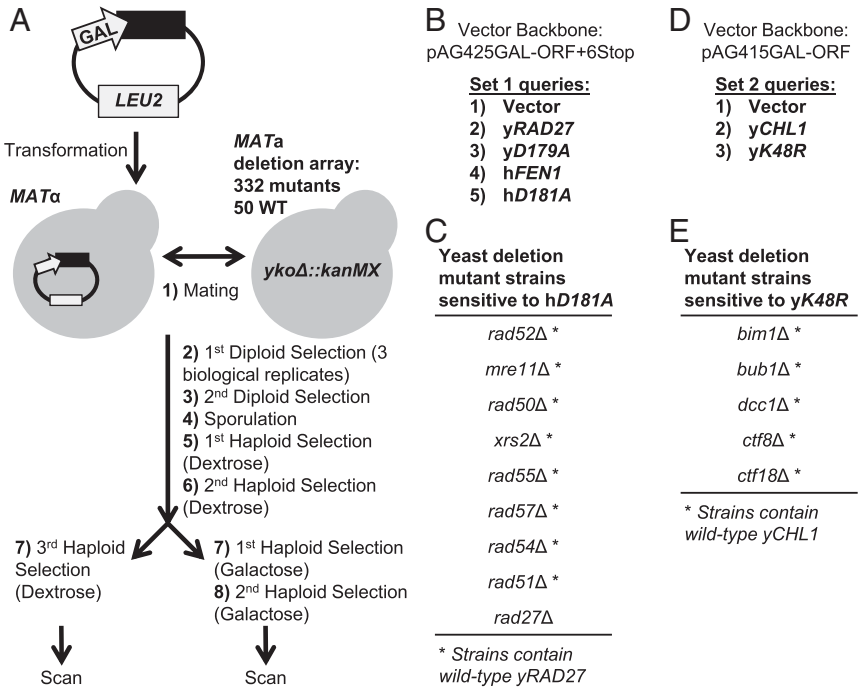

Fig. 1. Dominant mutations in h*FEN1* and y*CHL1* generate nonoverlapping dominant SL interaction networks. (*A*) Inducible yeast expression vectors or a vector control were transformed to generate query strains. Using SGA technology, each query strain was mated to a pinned miniarray comprising 332 haploid yeast knockouts and 50 wild-type (WT) strains to generate diploids. Following diploid selection (two rounds) and sporulation, a series of replica-pinning steps generated a haploid array where each knockout mutant was combined with the expression vector. After two rounds of haploid selection, strains were pinned onto galactose media (two rounds) to induce expression of the ORF. The final plates were scanned (*SI Appendix*, Fig. S1), and the area of each pinned spot was determined to detect dominant SL interactions. (*B*) The first set of vectors comprised wild-type yeast *RAD27* or human *FEN1*, along with the corresponding nuclease-defective mutants, yeast *rad27-D179A*, or human *FEN1-D181A*, respectively. (*C*) Validated list of yeast deletion mutant strains that are sensitive to expression of h*FEN1-D181A*. Validations are shown in *SI Appendix*, Fig. S2. (*D*) The second set of vectors comprised wild-type yeast *CHL1* or the corresponding helicase-deficient yeast *chl1-K48R* mutant. (*E*) Validated list of yeast deletion mutant strains that are sensitive to expression of *chl1-K48R*.

Nuclease-Defective hFEN1 Induces DNA Damage in a Dominant Manner. We identified the HR proteins as required to tolerate the dominant effects of hD181A on cell growth (Fig. 2 and *SI Appendix*, Figs. S2 and S3). Given that the HR pathway is responsible for repairing DNA double-strand breaks (32), these results suggested that ectopic expression of dominant h*FEN1-D181A* mutations generated DNA damage. To test this hypothesis, we measured the frequency of yRad52 foci in these cells as an indicator of DNA damage. We generated humanized hetero-allelic haploids whereby two alleles of the h*FEN1* ORFs were integrated into a haploid strain at the y*RAD27* and y*URA3* genomic loci, both under the transcriptional control of the y*RAD27* promoter. Hetero-allelic haploid strains expressing both h*FEN1* and h*FEN1-D181A* had increased Rad52-GFP foci compared to a strain expressing two copies of h*FEN1* (Fig. 3*A*).

Nuclease-Defective hFEN1 Causes Dominant Sensitivity to MMS-Induced DNA Damage. FEN1 has a role in repairing DNA damage. To determine if the nuclease-defective hD181A mutant protein could block DNA repair in vivo, we exposed hetero-allelic haploids expressing both h*FEN1* and h*FEN1-D181A* or two copies of h*FEN1* to the alkylating agent, MMS. The hetero-allelic haploid strain expressing h*FEN1-D181A* was sensitive to MMS treatment (Fig. 3*B*). This result was confirmed with heterozygous diploid strains expressing endogenously-regulated genomic copies of the h*FEN1* ORFs that have been integrated at the y*RAD27* loci (*SI Appendix*, Fig. S4).

Dominant SL of Inactive hFEN1 with HR Mutants Is Dependent on DNA Binding. One potential explanation for the dominant SL observed in HR-deficient cells is that the nuclease-defective hD181A protein, which can block wild-type hFEN1 DNA binding in in vitro competition assays (24, 25), could also block wild-type hFEN1 DNA binding in yeast cells. Blockage of the wild-type enzyme by a nuclease-defective mutant protein would result in nonprocessed DNA substrates that ultimately lead to DNA damage and a requirement for HR-mediated repair. We reasoned that, if we disrupted the DNA-binding ability of the hD181A mutant protein, we would suppress the dominant SL. We tested a panel of eight candidate DNA-binding mutations for suppression of the dominant SL phenotype. Data from in vitro DNA enzymatic/binding assays showed that hR47A, hR70A, hR103A/R104A, hK128A/R129A, and hK200A had reduced nuclease and DNA-binding activities while hR192A, hK201A, and hK252A/K254A had no detectable nuclease activities or DNA-binding affinities (31). The hR47A and hR70A mutations were also shown by in vitro competition assays to partially suppress the ability of a hD181A mutant protein to block wild-type hFEN1 substrate processing (33).

We ectopically expressed each human DNA-binding mutant allele, alone or in combination as double mutants with h*FEN1-D181A*, in a humanized *rad27*Δ::h*FEN1* yeast strain that is y*RAD52*-deficient, and assessed the effect of the putative DNA-binding mutations on the dominant SL. Four mutants (hR47A, hR70A, hR103A/R104A, and hK128A/R129A) partially suppressed the h*FEN1-D181A* dominant SL with *rad52*Δ (Fig. 4 *A* and *B* and *SI Appendix*, Figs. S5 and S6). Our in vivo experiments demonstrate the applicability of the results observed for hR47A and hR70A using in vitro competition assays (33) and further expanded the list with two additional DNA-binding mutants that partially suppress hD181A protein binding capabilities.

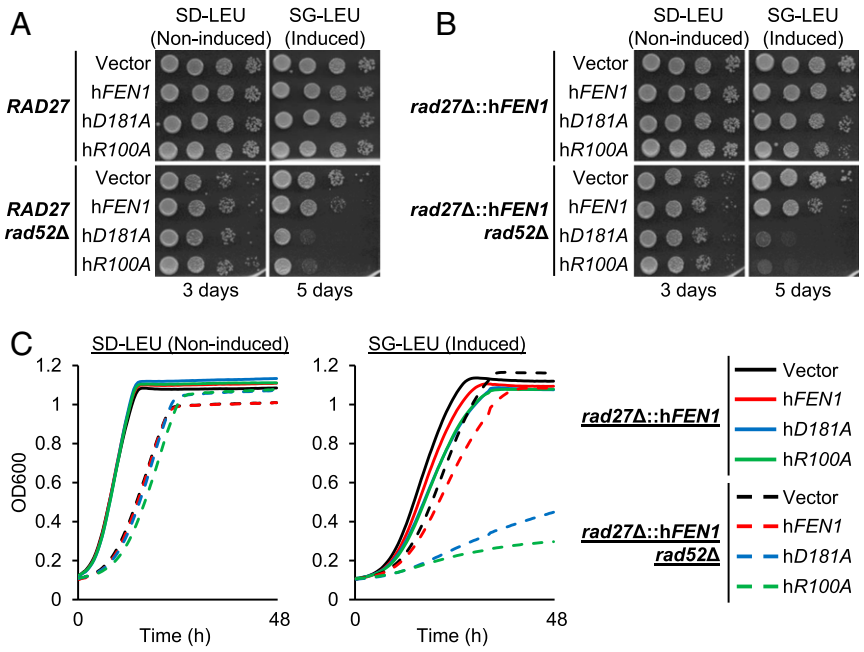

Fig. 2. Nuclease-defective h*FEN1* mutations cause dominant SL with HR-defective mutants. Expression of nuclease-defective h*FEN1* mutants h*FEN1-D181A* and h*FEN1-R100A* cause growth defects in a *rad52*Δ mutant strain containing either (*A*) endogenous wild-type y*RAD27* or (*B*) wild-type h*FEN1* that has replaced genomic y*RAD27*. (*C*) The observed growth defects were validated by liquid growth curve assays. Each represented curve is the average of three replicates. Validation using liquid growth assays for *A* and quantification of strain fitness for all growth curves are shown in *SI Appendix*, Fig. S3.

Since these four mutants retained some nuclease and DNA-binding activity in vitro (31), we tested whether these mutations could partially rescue hD181A nuclease activity. We utilized in vivo cross-species complementation assays to determine the functional status of the human DNA-binding mutants (34). Strains deficient in y*RAD27* are sensitive to MMS treatment, and ectopic expression of h*FEN1* can complement this sensitivity (29). The dominant nuclease-defective mutants hD181A and hR100A caused severe fitness defects in a *rad27*Δ mutant and were unable to complement *rad27*Δ sensitivity to MMS (Fig. 5*A*). In contrast, all eight human DNA-binding mutants partially complemented *rad27*Δ sensitivity to MMS (Fig. 5*B* and *SI Appendix*, Fig. S7), suggesting that these mutants have reduced activity in vivo. However, when combined with hD181A, the DNA-binding mutations could not suppress *rad27*Δ sensitivity to MMS, demonstrating that the DNA-binding mutations did not restore activity to a hD181A mutant protein (Fig. 5*B* and *SI Appendix*, Fig. S7). Western blot analysis demonstrated that the introduction of DNA-binding mutations did not affect hD181A protein stability (*SI Appendix*, Fig. S8). Taken together, these results indicate that the suppression of the *rad52*Δ h*FEN1-D181A* dominant SL by the DNA-binding mutations (hR47A, hR70A, hR103A/R104A, and hK128A/R129A) is not a result of restored nuclease activity or decreased protein stability. These results are consistent with a model of a hFEN1–DNA cytotoxic complex that leads to DNA damage requiring HR-mediated repair.

Helicase-Deficient yCHL1 Is Dominant SL with Spindle-Associated and Ctf18-RFC Mutants, but Not HR Mutants. To test whether other replisome-associated proteins could be mutated to cause dominant SL in a manner similar to h*FEN1-D181A,* we targeted the yeast Chl1 helicase. yChl1/hDDX11 interacts with several replisome-associated proteins, including FEN1 (35–37). A conserved lysine-to-arginine substitution has previously been described in both yChl1 (K48R) and hDDX11 (K50R). This mutation abolishes helicase activity of both yChl1 (37) and hDDX11 proteins (38, 39) but retains hDDX11 binding to DNA in vitro (39) and recruitment to the replication fork in yeast (37). Chromosome transmission fidelity (CTF) assays demonstrated that expression of the yeast *chl1-K48R* allele resulted in a dominant effect on chromosome stability (40). Unlike *yRAD27*, galactose-inducible expression of wild-type y*CHL1* or the dominant *chl1-K48R* allele did not cause severe growth defects in wild-type yeast (*SI Appendix*, Fig. S1) and were therefore utilized as queries for SGA screening (Fig. 1*D*).

None of the 332 mutants on the SGA miniarray exhibited reduced growth upon induced ectopic expression of y*CHL1*, indicating that elevated levels of the wild-type protein are tolerated in all of the 332 yeast deletion strains tested (Dataset S3). We identified 59 putative dominant SL interactions that displayed >20% growth defects upon ectopic expression of *chl1-K48R* (Dataset S4). We selected the top negative interactions for testing by liquid growth assays and validated the *chl1-K48R* dominant SL with 4 mutants that are part of the spindle-associated and checkpoint (SAC) pathway (y*BUB1*, y*BIM1*), and the Ctf18–RFC complex (y*DCC1* and y*CTF8*) (Fig. 1*E* and Dataset S4).

Given that both y*CHL1* and the interacting genes are required for chromosome maintenance, which could affect plasmid segregation and stability, we constructed hetero-allelic haploids by integrating galactose-inducible yeast *CHL1* or the *chl1-K48R* alleles at the *URA3* locus, in a strain containing y*CHL1* at the endogenous locus. We retested the previously validated mutants (*bub1*Δ, *bim1*Δ, *dcc1*Δ, and *ctf8*Δ), as well as additional mutants of interest (Dataset S4), and confirmed the dominant SL that occurs upon induction of *chl1-K48R* (Fig. 6*A* and *SI Appendix*, Fig. S9). The Ctf18–RFC is a complex comprised of RFC2-5 (common to all RFC complexes) as well as three unique genes (y*DCC1*, y*CTF8*, and y*CTF18*) (41, 42). As we identified two of three unique Ctf18-RFC genes in our screen, we directly tested *ctf18*Δ and confirmed that expression of *chl1-K48R* also causes a dominant SL effect in this mutant (Fig. 6*B* and *SI Appendix*, Fig. S9).

In contrast to h*FEN1-D181A*, expression of the yeast *chl1-K48R* allele was not dominant SL with *rad52*Δ (*SI Appendix*, Fig. S9 and Dataset S4), suggesting that the mechanism underlying dominant SL is different between h*FEN1* and y*CHL1*. Furthermore, and in

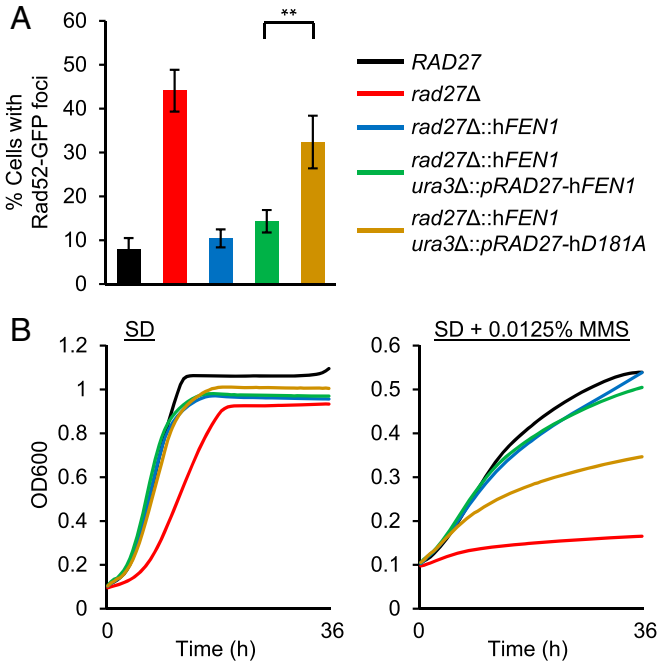

Fig. 3. Nuclease-defective h*FEN1* induces DNA damage and sensitivity to MMS in a dominant manner. (*A*) Yeast hetero-allelic haploids containing genomic copies of h*FEN1* and h*FEN1-D181A*, and under control of the same y*RAD27* promoter, have increased Rad52-GFP foci. Four replicate experiments were performed, and a minimum of 200 cells were counted per replicate (mean ± SD). Student's *t* test. $^{**}P < 0.01$. (*B*) The same strains were assessed for growth defects in the presence of the DNA-damaging agent MMS. Each represented curve is the average of three replicates. Quantification of strain fitness is shown in *SI Appendix*, Fig. S4.

agreement with previous studies (37), expression of *chl1-K48R* did not confer growth defects in a *chl1*Δ mutant (*SI Appendix*, Fig. S9). This is in contrast to the severe growth defects observed for a *rad27*Δ mutant that contains inactive hD181A protein (Fig. 5*A*).

The Effect of DNA- or Replisome-Binding Mutations on the yCHL1 Dominant SL Is Dependent on the SL Partner Mutation. To test whether DNA or replisome binding was critical for dominant SL with *chl1-K48R*, we tested several mutations that have previously been identified to disrupt the replisome or DNA binding of yChl1/hDDX11. Yeast Chl1 binds the replisome through a protein–protein interaction with yCtf4, and it has been shown that a DDIL-to-DAIA mutation in yChl1, which disrupts the Ctf4-interacting-peptide (CIP-box) motif, abrogates this binding (37). A glutamine-to-alanine mutation at a conserved residue in the Q-motif of hDDX11 (hQ23A or yQ20A) abolished the DNA-binding ability of the purified human protein in vitro (43).

Using the same inducible hetero-allelic system in which various y*CHL1* constructs are integrated at the *URA3* locus (in the presence of endogenously regulated wild-type y*CHL1*), we expressed the replisome-binding (*chl1-DAIA*) and putative DNA-binding (*chl1-Q20A*) mutants alone, or in combination with yK48R (*chl1-K48R/DAIA* or *chl1-Q20A/K48R*), or as a triple mutant (*chl1-Q20A/K48R/DAIA*) in the genetic backgrounds in which the dominant SL effect was observed. Introduction of these mutations in different combinations did not affect the stability of the yChl1 protein (*SI Appendix*, Fig. S10). Expression of the two binding mutations alone (*chl1-Q20A* or *chl1-DAIA*), or together (*chl1-Q20A/DAIA*), did not result in a dominant effect on growth (Fig. 6 and *SI Appendix*, Fig. S9). The dominant SL caused by *chl1-K48R* expression in the spindle-associated mutants was suppressed by introduction of both the replisome-binding and DNA-binding mutations (separate or together). In contrast, in the Ctf18-RFC mutated strains, the *chl1-K48R* dominant SL was not suppressed by introduction of either or both of the binding mutations, suggesting that the mechanism of dominant SL varies between these two pathways (Fig. 6*B* and *SI Appendix*, Fig. S9).

Helicase-Deficient yCHL1 Is Dominant SL with Cohesin Mutants. Yeast *chl1*Δ mutant cells exhibit increased rates of chromosome instability (44), as well as sister chromatid cohesion defects (37, 45, 46). The deletion mutants identified in the screen as SL with dominant *chl1-K48R* also display defects in chromosome stability or sister chromatid cohesion (42, 45, 47). CTF assays, which

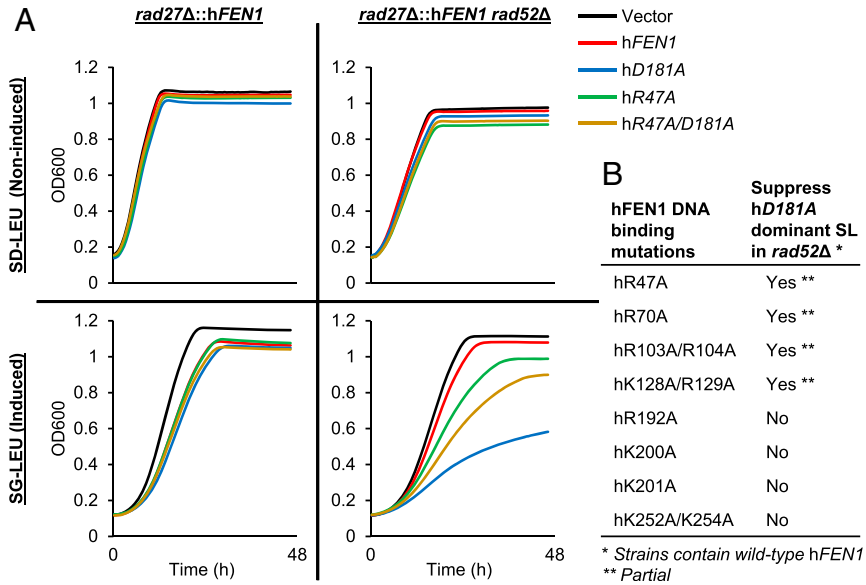

Fig. 4. DNA-binding mutations suppress the dominant SL of nuclease-defective h*FEN1* with HR-defective mutants. (*A*) The hFEN1 DNA-binding mutant hR47A partially suppresses fitness defects of *rad52*Δ mutant strains expressing nuclease-defective h*FEN1-D181A*. Each represented curve is the average of three replicates. (*B*) Summary of hFEN1 DNA-binding mutations tested in this study. Corresponding liquid growth assays for each mutant are shown in *SI Appendix*, Fig. S5. Quantification of strain fitness for all DNA-binding experiments is shown in *SI Appendix*, Fig. S6.

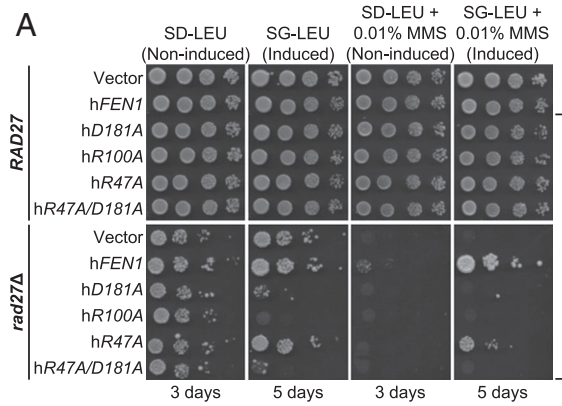

B

hFEN1 DNA binding mutations	Rescue *rad27Δ* sensitivity to MMS	Suppress *rad27Δ* sensitivity to h*D181A*
hR47A	Yes *	No
hR70A	Yes *	No
hR103A/R104A	Yes *	No
hK128A/R129A	Yes *	No
hR192A	Yes *	No
hK200A	Yes *	No
hK201A	Yes *	No
hK252A/K254A	Yes *	No

* *Partial*

Fig. 5. Human *FEN1* DNA-binding mutations partially complement *rad27*Δ but cannot rescue hD181A loss of function. (*A*) The hFEN1 DNA-binding mutant hR47A partially complements *rad27*Δ sensitivity to MMS. The nuclease-defective hD181A causes severe fitness defects in the absence of yRad27, and these defects cannot be suppressed by hR47A. (*B*) Summary of hFEN1 DNA-binding mutations tested in this study. Corresponding growth assays for each mutant are shown in *SI Appendix*, Fig. S7.

measure loss of artificial chromosomes, revealed a dominant effect of *chl1-K48R* on chromosome stability (40). We confirmed this effect using an alternative assay that measures loss of an endogenous genomic locus. Using the a-like faker (ALF) assay (48), we demonstrated that expression of the *chl1-K48R* allele in the presence of wild-type y*CHL1* increased genome instability (*SI Appendix*, Fig. S11).

Knockout mutants of y*CHL1*, spindle-associated genes, and Ctf18–RFC complex genes are SL with mutations in cohesin genes (20, 49). We tested whether *chl1-K48R* was dominant SL with mutations affecting the cohesion pathway. The cohesin complex is comprised of four essential core proteins (ySmc1, ySmc3, yScc1, yIrr1) that are loaded onto DNA by a separate complex composed of yScc2 and yScc4 (50). As these are essential genes, we selected temperature-sensitive mutants of core (*smc1-259* and *scc1-73*) and loader (*scc2-4*) subunits and examined the effect of inducible expression of y*CHL1* or *chl1-K48R* on growth. Expression of *chl1-K48R*, in the presence of wild-type y*CHL1*, caused severe growth defects in all three cohesin mutants (Fig. 7*A* and *SI Appendix*, Fig. S12), indicating a dominant SL interaction with mutations in the cohesion pathway. However, *chl1-K48R* does not exhibit dominant SL with all cohesion mutants. For example, the nonessential cohesin accessory subunit, yRad61, also functions in the cohesion pathway. The *rad61*Δ mutant did not meet the cutoff in our *chl1-K48R* dominant SL screen (Dataset S4). To determine if this was a false-negative hit, we directly tested the effect of *chl1-K48R* expression on fitness of a *rad61*Δ mutant strain and determined

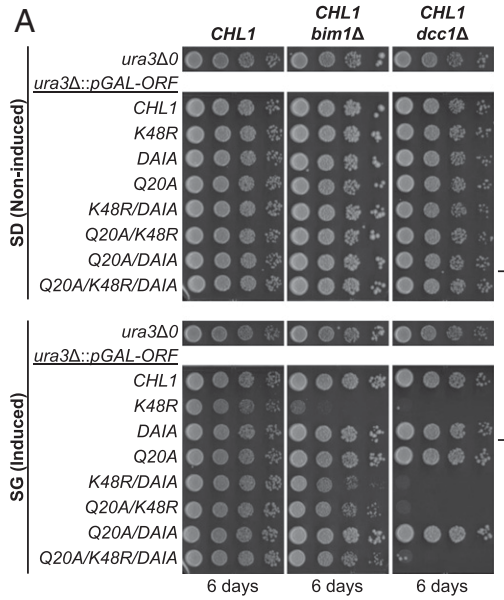

B

Yeast deletion mutant strains sensitive to y*K48R* *	Dominant SL suppressed by DAIA (replisome binding mutation)	Dominant SL suppressed by Q20A (DNA binding mutation)
*bim1*Δ **	Yes	Yes
*bub1*Δ **	Yes	Yes
*dcc1*Δ ***	No	No
*ctf8*Δ ***	No	No
*ctf18*Δ ***	No	No

* *Strains contain wild-type yCHL1*
** *Spindle-associated*
*** *Ctf18-RFC complex*

Fig. 6. Helicase-deficient y*CHL1* causes dominant SL with spindle-associated and Ctf18–RFC complex mutants. (*A*) Yeast hetero-allelic haploids, containing a genomic copy of endogenously regulated y*CHL1*, were generated by integrating galactose-inducible ORFs at the *URA3* locus. Inducible expression of the helicase-deficient y*CHL1* mutant *chl1-K48R* causes dominant SL in spindle-associated *bim1*Δ and Ctf18-RFC subunit *dcc1*Δ mutant strains. The replisome-binding mutant (yDAIA) and putative DNA-binding mutant (yQ20A) can suppress (separate or together) the dominant SL observed in the *bim1*Δ strain. The same mutants (separate or together) are unable to suppress the dominant SL observed in the *dcc1*Δ strain. (*B*) Summary of *chl1-K48R* dominant SL interactions identified in this study. The dominant SL observed in the spindle-associated mutants can be suppressed by both replisome- and DNA-binding mutations while the dominant SL observed in the Ctf18–RFC complex mutants cannot be suppressed by either binding mutations. Corresponding growth assays are shown in *SI Appendix*, Fig. S9.

that expression of this allele was not dominant SL in this mutant background (*SI Appendix*, Fig. S12).

We combined the K48R mutant with the replisome-binding (DAIA) and/or DNA-binding (Q20A) mutations. In the strains bearing mutations in the cohesin core subunits (*smc1-259* and *scc1-73*), the *chl1-K48R* dominant SL interaction was suppressed by the Q20A and DAIA mutants. In contrast, the property of *chl1-K48R* dominant SL with the cohesin loader mutation (*scc2-4*) was not suppressed by either the Q20A or the DAIA mutants. Instead, expression of the *chl1-Q20A/DAIA* allele caused dominant growth defects in the *scc2-4* mutant (Fig. 7 *A* and *B*). Together, these results indicate that dominant SL may be able to separate the functional differences between members of the same biological pathway. When compared to the hFEN1-DNA cytotoxic lesions that cause DNA damage, our results suggest the formation of yChl1-DNA and/or yChl1-protein cytotoxic lesions that have varying effects on DNA-associated processes.

Discussion

Many chemotherapeutics, such as intercalators, DNA cross-linkers, and alkylating agents, bind directly to DNA and modify DNA function by inducing damage or by blocking replication and/or transcription (51). In a similar manner, proteins can be trapped on DNA, leading to cytotoxic intermediates that induce damage and affect replication and/or transcription mechanisms (11). Even a small amount of protein trapped on DNA could result in cytotoxic intermediates that require processing or trigger a checkpoint response and as a result cause differential killing in repair- or checkpoint-response mutants relative to wild-type. Given that a trapping inhibitor would not need to completely abolish all activity to be effective, protein trapping could provide a means for targeting essential proteins, such as topoisomerases and FEN1. In this way, trapping inhibitors that trap proteins could effect dominant SL with mutations affecting the DNA damage response. Here, we demonstrated that certain inactivating mutations in h*FEN1* or y*CHL1* elicit dominant SL with mutations affecting replication fidelity and the DNA damage response.

SL and dominant SL interactions identify candidate drug targets and genetic backgrounds that can be selectively targeted by inhibitors. In the case of hFEN1, knockout-based SL screens of *rad27*Δ identify a much larger and broader genetic interaction network than the dominant SL network identified in this study (*SI Appendix*, Fig. S13). This demonstrates that genetic interaction networks generated from knockout/knockdown mutants may differ from the genetic interaction networks of dominant inhibited proteins. While the *rad27*Δ knockout mutant requires HR and numerous other pathways, the dominant mutant form of the hFEN1 protein is only SL with HR mutants, which is consistent with the formation of a cytotoxic hFEN1–DNA substrate complex. In contrast, the dominant mutant form of yChl1 was not SL with HR mutants even though some of the dominant SL interactions are dependent on DNA binding. The expression of dominant mutant forms of h*FEN1* and y*CHL1* result in strikingly different genetic dependencies. Cells expressing a dominant mutant form of y*CHL1* exhibited a more complex dependency pattern and were dependent on replication fork mediators, such as the Ctf18–RFC and the cohesin complex as well as the proteins associated with mitotic spindle assembly. The multiple genetic dependencies of a dominant helicase-deficient yChl1 are reflective of the fact that yChl1 is a nexus for replication, repair, and sister chromatid cohesion and has many genetic and physical interactions (16, 37, 52). The complexity of these dominant SL interactions is also evident in the suppressive effects of the mutations in the DNA- and Ctf4-binding domains. The mutations affecting the DNA- and Ctf4-binding domains suppressed the dominant SL with the spindle-associated mutations but not the Ctf18-RFC mutations (Fig. 6) and suppressed the dominant SL with the core cohesin mutations but not the cohesin loader mutations (Fig. 7). This suggests that, unlike hFEN1, at least some of the dominant SL interactions are not dependent on direct DNA binding. It is possible that the dominant SL with the

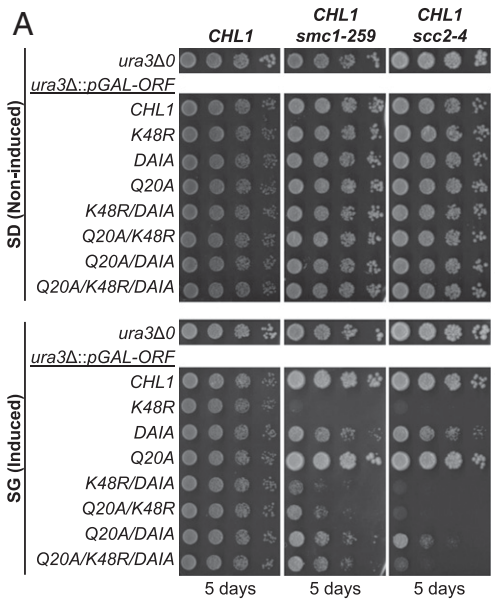

B

Yeast cohesin mutant strains sensitive to y*K48R* *	Dominant SL suppressed by DAIA (replisome binding mutation)	Dominant SL suppressed by Q20A (DNA binding mutation)
smc1-259 **	Yes	Yes
scc1-73 **	Yes	Yes
scc2-4 ***	No	No

* *Strains contain wild-type yCHL1*
** *Cohesin core subunits*
*** *Cohesin loader subunit*

Fig. 7. Helicase-deficient y*CHL1* causes dominant SL with cohesin mutants. (*A*) Yeast hetero-allelic haploids, containing a genomic copy of endogenously regulated y*CHL1*, were generated by integrating galactose-inducible ORFs at the *URA3* locus. Inducible expression of the helicase-deficient y*CHL1* mutant *chl1-K48R* causes dominant SL in the cohesin core, *smc1-259*, and cohesin loader, *scc2-4*, temperature-sensitive mutant strains. The replisome-binding mutant (yDAIA) and putative DNA-binding mutant (yQ20A) can suppress (separate or together) the dominant SL observed in the cohesin core mutant strain, but not the loader mutant strain. (*B*) Summary of *chl1-K48R* dominant SL interactions with cohesin mutants tested in this study. Corresponding growth assays are shown in *SI Appendix*, Fig. S12.

Ctf18-RFC and cohesin loaders is due to direct interactions between these proteins and the mutant form of yChl1. The human yChl1 ortholog, DDX11, physically interacts with the Ctf18-RFC (35), and yChl1 regulates the deposition of the cohesin loaders on DNA during S-phase (53). The dominant mutant form of yChl1 could affect replication without directly interacting with DNA by binding to and impeding the Ctf18-RFC or cohesin loaders. It is also interesting to note that the helicase activity of yChl1 is not required for sister chromatid cohesion (37), demonstrating that it is possible to inhibit some functions of a protein while retaining other essential functions. DNA and RNA helicases constitute a large class of potential therapeutic targets. It has been proposed that catalytically inactive helicases could bind DNA and block access to replication and repair factors (54). EIF4A inhibitors have been discovered that trap the helicase on its RNA substrate (55) demonstrating that helicases can be inhibited to generate toxic inhibitor–protein–substrate complexes.

Most large-scale genetic interaction screens have utilized knockout or knockdown approaches (3). However, many DNA damage response genes are essential or are multifunctional, limiting the efficacy of CRISPR- or RNAi-based genetic approaches to study genetic interactions. Missense mutations can be used to deduce structural and functional information about proteins (56) and can mimic the effect of protein inhibitors (13). To determine if the SL targets, hFEN1 or yChl1, could be trapped on DNA and create a cytotoxic lesion, we generated inactivating mutations that did not affect DNA binding or protein stability. In this way, we mimicked the predicted effect of inhibitors that induce dominant cytotoxic complexes by inhibiting protein activity without affecting binding to DNA substrates. Subsequently, we used additional missense mutations to disrupt DNA- and protein-binding domains in conjunction with the inactivating mutations to determine whether DNA or protein binding were required for the dominant effects observed for catalytically inactive hFEN1 and yChl1. Unbiased high-throughput screening of mutations in candidate trapping proteins, such as deep mutational scanning (56), would reveal sites that are mutable to a dominant SL phenotype. Structural analysis of these mutations within DNA-binding proteins (57) could then be used to design new inhibitors that mimic the structural changes and elicit target trapping. Recently, Zandarashvili et al. demonstrated the viability of this approach by combining mutational analysis and structural data to modify a nontrapping PARP inhibitor, veliparib, to a PARP-trapping form (58). While it may not be possible to directly mimic the structural changes induced by dominant mutations using small molecules, the mutation may identify protein regions that could be targeted with small molecules to cause protein trapping.

To date, research into the development of hFEN1 inhibitors has mostly focused on the series of *N*-hydroxyurea–based compounds (59). These compounds have been shown to selectively impair proliferation of HR-defective cancer cell lines (60–62), thereby confirming the SL interaction between *rad27*Δ and HR mutants. While most inhibitors in this series are substrate-competitive inhibitors that bind free hFEN1, one has been shown to have affinity for both DNA-free and DNA-bound forms of hFEN1, resulting in a "dead-end" enzyme–inhibitor–substrate complex (60). Our genetic results suggest that this complex may be a cytotoxic lesion and that some of the SL observed with HR-defective cancer cell lines treated with this inhibitor could be attributed to a dominant effect. To date, there has been no report of uncompetitive hFEN1 inhibitors, which bind only to the enzyme–substrate complex (23). In pursuit of these trapping inhibitors, dominant SL assays can direct structure-based rational drug design. Our study found that the four DNA-binding mutations that partially suppress dominant SL of nuclease-defective hFEN1 with HR mutants lie in the helical gateway, helical cap, and hydrophobic wedge domains (63, 64). In contrast, the four DNA-binding mutations that fail to suppress the dominant SL of nuclease-defective hFEN1 with HR mutants are located in the β-pin and H2TH motifs (63, 64). These results implicate hFEN1 DNA-binding interfaces that are required for maintaining a cytotoxic enzyme–inhibitor–substrate complex. Dominant SL could be exploited in cell-based platforms for high-throughput screening of trapping inhibitors. Experimental evidence indicates that 1) the *N*-hydroxyurea–based compounds are species-specific based on in vitro (60) and in vivo (29) studies; 2) hFEN1 can complement yRad27 (27, 29); and 3) the inhibitors can selectively induce growth defects in a humanized *rad27*Δ::h*FEN1* yeast strain that is HR-deficient (29). Based on these parameters and the results of this study, only a trapping inhibitor would elicit dominant SL in an HR-deficient strain that is ectopically expressing wild-type h*FEN1* in the presence of y*RAD27*.

While catalytically inactivating mutations have great potential to cause trapping, it is probable that other missense mutations could also result in trapping and dominant SL and potentially be more efficacious. Many DNA damage responses are controlled by posttranslation modifications. For example, the PARylation of DNA-bound PARP promotes allosteric changes that cause the dissociation of PARP from DNA (4, 58). Mutations affecting phosphorylation, ubiquitination, SUMOylation, or protein–protein interaction sites could result in trapped cytotoxic protein intermediates. Our study shows the potential to generate genetic interaction networks with missense mutations rather than gene knockouts. In turn, these dominant SL interactions will help select more effective targets, suggest mechanisms underlying SL interactions, and direct small molecule screening approaches to identify compounds that more effectively phenocopy the SL effect. This approach will increase the chance that SL targets translate into effective therapies.

Materials and Methods

Dataset S5 lists plasmids, strains, and primers used in study.

Expression Vectors. Human *FEN1* in an entry clone was obtained from hORFeome V8.1 (65). Yeast *RAD27* and *CHL1* from the Gateway-compatible FLEX array (66) were shuttled to a donor vector to generate entry clones using BP Clonase II (Invitrogen). Missense mutations were introduced in the entry clones using the QuikChange Site-Directed Mutagenesis Kit (Agilent) and verified by Sanger sequencing. Wild-type and mutant y*RAD27* or h*FEN1* entry clones were then shuttled into the yeast destination vector pAG425GAL-ccdB+6Stop (*LEU2*, 2μ, inducible GAL promoter, 6-amino acid C-terminal extension) (67, 68) using LR Clonase II (Invitrogen) to generate expression vectors. Wild-type and mutant y*CHL1* entry clones were shuttled into the yeast destination vector pAG415GAL-ccdB (*LEU2*, CEN, inducible GAL promoter) (67).

Gateway-compatible *ura3*-integration vectors (two versions) were constructed by modifying pWS1291 (containing homology upstream and downstream to the *ura3Δ0* locus and flanked by NotI digestion sites) (gift from Tom Ellis, Imperial College London, London, United Kingdom). The yeast *LEU2* cassette was PCR amplified from pRS415 (69) using primers (OPH9725 and 9726) and cloned between PstI and SpeI sites to create a yeast selectable version of pWS1291. To convert pWS1291 and pWS1291_LEU2 to Gateway-compatible plasmids, the origins of replication and bacterial selection markers were replaced with those from pAG415GAL-ccdB (67) using a PCR-amplified fragment (primers OPH9834 and 9835) that was cloned between the NotI sites in pWS1291 and pWS1291_LEU2. Another PCR product containing the *GAL1/10* promotor, ccdB cassette, and C-terminal 3xHA tag was amplified using primers (OPH9727 and 9728) and cloned between the BmgBI sites. Correct orientation of inserts was verified by PCR and sequencing. The resultant vectors, pLA581 (ura3_int_GAL-ccdB-HA_LEU2) and pLA575 (ura3_int_GAL-ccdB-HA), were used to integrate ORFs into the *ura3Δ0* locus.

Yeast Strains. The miniarray was constructed by repinning 332 nonessential yeast knockout strains from the Deletion Mutant Array (DMA) collection (70). Each *MAT*a haploid yeast knockout, marked by *kanMX*, was verified by PCR. The corresponding yeast proteins function in DNA-related pathways and mostly have conserved human homolog(s). Fifty *MAT*a wild-type (*his3*Δ1::*kanMX*) spots were pinned randomly in the array as control strains.

For h*FEN1* experiments, expression vectors and the vector control pRS425 (*LEU2*) (71) were transformed into wild-type and mutant yeast strains obtained from the miniarray. Vectors were also transformed into humanized

*MAT*a *rad27*Δ::h*FEN1* (+/− y*RAD52*) strains that were constructed previously (29). Transformants were selected on SD−Leu (synthetic medium plus 2% dextrose and lacking leucine). Hetero-allelic humanized haploids were constructed using the *MAT*a *RAD52-GFP* strain from the yeast GFP collection (72). The GFP-tagged strain was modified using CRISPR/Cas9-mediated deletion of y*RAD27* and CRISPR/Cas9-mediated replacement of y*RAD27* with the h*FEN1* ORF as previously described (29). To integrate the h*FEN1* or h*FEN1-D181A* ORFs at the *ura3Δ0* locus, attB-flanked PCR products (primers OMD295 and 297) containing the y*RAD27* promoter and the human ORFs (designed to include stop codons) were shuttled to a donor vector to generate entry clones using BP Clonase II. The entry clones were then shuttled to pLA575 using LR Clonase II to generate integration vectors. Following NotI digestion, a CRISPR/Cas9-mediated integration of the linearized vectors into the *ura3Δ0* locus (guide: TCAGGGTCCATAAAGCTCCC) was performed to generate the hetero-allelic haploids. Humanized *MAT*a/α heterozygous diploid strains were constructed using the previously described strain *MAT*a *rad27*Δ::h*FEN1* and the similarly constructed *MAT*a *rad27*Δ::h*FEN1-D181A*. A CRISPR/Cas9-mediated mating type switch converted the *MAT*a haploids into *MAT*α haploids as previously described (73). Diploids were constructed by isolating zygotes following mating of the *MAT*a and *MAT*α humanized haploids.

For y*CHL1* experiments, wild-type and mutant y*CHL1* ORFs (containing stop codons) were shuttled from entry clones to pLA581 using LR Clonase II. Following NotI digestion, the galactose-inducible ORFs were integrated into the *ura3Δ0* locus by transformation of the linearized vectors into the strain (Y7092) (*MAT*α *can1*Δ::*STE2pr-his5 lyp1*Δ *ura3Δ0 leu2Δ0 his3Δ1 met15Δ0*) and selection of transformants on SD−Leu medium. Correct integration was confirmed by PCR. These hetero-allelic haploids were then mated to *MAT*a *kanMX*-marked deletion (from the miniarray) and *URA3*-marked temperature-sensitive (20) strains. Diploids were selected and sporulated using the same methods described for the screen. Following sporulation, hetero-allelic haploids containing deletions or temperature-sensitive mutations were obtained by streaking to single colonies on haploid selection media SD−HRLK (−His −Arg −Leu −Lys + 50 μg/mL canavanine + 50 μg/mL thialysine + 2% dextrose) containing either 200 μg/mL G418 (for deletion strains) or lacking uracil (for temperature-sensitive strains). Hemagglutinin (HA)-tagged strains were constructed using the hetero-allelic haploids by removing the stop codons and bringing the 3xHA tag in-frame with the ORFs. The CRISPR/Cas9 protocol utilized a guide RNA (gRNA) targeted to the linker region between the ORF and the 3xHA tag (guide: AATTCGATATCAAGCTTAGG). Donor DNA was constructed by annealing two complimentary oligos composed of flanking homology to the left and right of the integration site (primers OPH9879 and 9880).

Dominant SL Screens. Galactose-inducible expression vectors and the vector controls pRS425 (*LEU2*, 2μ) or pRS415 (*LEU2*, CEN) were transformed into the SGA-starter strain (Y7092), and transformants were selected on SD−Leu medium. Query strains (Y7092) containing *LEU2*-marked vectors were crossed to the miniarray using SGA technology (74). A series of replica-pinning steps using a Singer RoToR robot generated an array of deletion mutants on dextrose media containing either a vector control or the expression plasmids, which were induced by pinning onto media containing galactose. Initially, query strains were grown to saturation in triplicates in SD−Leu before plating on the same media to generate lawns of cells. Query strains were mated to the miniarray on yeast extract, peptone, and dextrose (YPD), and diploids were selected on SD−Leu+G418 (200 μg/mL) by two rounds of pinning. Diploids were pinned on sporulation medium (+ 50 μg/mL G418) and incubated for 7 d at 25 °C. Haploids were selected on SD−HRLK + drugs (−His −Arg −Leu −Lys + 50 μg/mL canavanine + 50 μg/mL thialysine + 200 μg/mL G418 + 2% dextrose) for two rounds before pinning on the same haploid selection plates containing either 2% dextrose or 2% galactose (two rounds of pinning on galactose). After the final plates were scanned, the area of each pinned spot was measured by Balony software (75) where the area of each deletion strain was normalized to the average area of all wild-type spots ($n = 50$) on the same plate. Interactions with a cutoff of >20% change in growth differential compared to the vector control plate were chosen for validation (experimental-control values <−0.2).

Yeast Assays. For spot assays, *LEU2*-marked strains (vector for h*FEN1* or integrated for y*CHL1* experiments) were serially diluted in 10-fold increments and plated (5 μL each spot) onto indicated media +/− chemicals. Spotting on SG−Leu (synthetic medium containing 2% galactose and lacking leucine) or SG (synthetic complete medium containing 2% galactose) induced expression of ORFs. For liquid growth assays, plasmid-bearing cultures were grown to midlog phase in −Leu selective medium containing either 2% dextrose or 2% galactose before diluting to optical density at 600 nm (OD_{600}) = 0.1 in 200 μL of the same medium +/− chemical. Plasmid-free cultures were grown in nonselective synthetic complete (SD) medium containing 2% dextrose to midlog phase before diluting to OD_{600} = 0.1 in 200 μL of the same medium +/− chemical. The 200-μL yeast cultures prepared in 96-well plates were loaded in a TECAN M200 plate reader, and OD_{600} readings were measured every 30 min over a period of 24 to 48 h. Before each reading, plates were shaken for 10 min. Each strain was tested in three replicates per plate per condition, and area under the curve (AUC) was calculated for each replicate. "Relative strain fitness" was defined as the AUC of each yeast strain curve relative to the AUC of the control strain curve grown on the same plate in the same medium condition. ALF assays were conducted as previously described (76). Growth assays involving temperature-sensitive strains were carried out at 25 °C while all remaining assays were conducted at 30 °C.

Whole Cell Extract and Western Blotting. Yeast cells were grown in inducing (2% galactose) or noninducing (2% dextrose) medium at 30 °C to midlog phase and harvested before resuspension of cell pellets in equal volume of Tackett Extraction Buffer [20 mM 4-(2-hydroxyethyl)-1-piperazineethanesulfonic acid (Hepes), pH 7.4, 0.1% Tween 20, 2 mM $MgCl_2$, 200 mM NaCl, protease inhibitors] (77). To lyse the cells, glass beads were added to the samples, and the mixture was vortexed in five 1-min blasts with 1-min incubation on ice between each vortex round. A 21-gauge needle (Becton Dickinson) was used to separate the crude whole cell extract from the beads into a new Eppendorf by poking a hole in the bottom of the tube and centrifuging at 1,000 rpm for 1 min. Lysates were cleared via centrifugation at 13,000 rpm for 15 min at 4 °C and normalized by protein concentration using the Bradford assay (Bio-Rad). Protein samples were subjected to sodium dodecyl sulfate polyacrylamide gel electrophoresis (SDS/PAGE) and Western blotting. Primary antibodies used included mouse anti-FEN1 (catalog no. NB100-150, 1:2,500; Novus), rabbit anti-FEN1 (catalog no. ab17994, 1:2,500; Abcam), mouse anti-HA (catalog no. ab18181, 1:1,000; Abcam), and mouse anti-PGK1 (Invitrogen, catalog no. 459250, 1:5,000). Secondary antibodies used were goat anti-mouse or anti-rabbit horseradish peroxidase (HRP) (1:10,000).

Microscopy. GFP-tagged strains were grown in SD complete medium at 25 °C to midlog phase. Live cells were immobilized on a Concanavalin A-coated glass slide and imaged using a Zeiss Axio Imager M2 microscope equipped with an ORCA-Flash4.0 LT+ Digital complementary metal oxide semiconductor (CMOS) camera (Hamamatsu) and a Zeiss Plan-Apochromat 100× oil immersion objective. Fluorescence images were acquired at 0.5-μm intervals along the *z* axis (total of 4.0-μm stack) by using Zeiss Zen2.3 pro software (blue edition). All z-stack images were max-projected for counting Rad52-GFP foci.

Data Availability. All study data are included in the article and/or supporting information.

ACKNOWLEDGMENTS. We thank Tom Ellis for providing plasmids used in this study. This work was supported by grants to P.H. from the Canadian Institutes of Health Research (CIHR) (MOP 38096 and FDN 148449) and the Canadian Cancer Society (CCSRI 704253). A.H. and L.A. were supported by doctoral awards from the CIHR and The University of British Columbia.

1. L. H. Hartwell, P. Szankasi, C. J. Roberts, A. W. Murray, S. H. Friend, Integrating genetic approaches into the discovery of anticancer drugs. *Science* **278**, 1064–1068 (1997).
2. M. Costanzo *et al.*, Global genetic networks and the genotype-to-phenotype relationship. *Cell* **177**, 85–100 (2019).
3. N. J. O'Neil, M. L. Bailey, P. Hieter, Synthetic lethality and cancer. *Nat. Rev. Genet.* **18**, 613–623 (2017).
4. B. A. Gibson, W. L. Kraus, New insights into the molecular and cellular functions of poly(ADP-ribose) and PARPs. *Nat. Rev. Mol. Cell Biol.* **13**, 411–424 (2012).
5. R. Krishnakumar, W. L. Kraus, The PARP side of the nucleus: Molecular actions, physiological outcomes, and clinical targets. *Mol. Cell* **39**, 8–24 (2010).
6. H. Farmer *et al.*, Targeting the DNA repair defect in BRCA mutant cells as a therapeutic strategy. *Nature* **434**, 917–921 (2005).
7. H. E. Bryant *et al.*, Specific killing of BRCA2-deficient tumours with inhibitors of poly(ADP-ribose) polymerase. *Nature* **434**, 913–917 (2005).
8. J. Murai *et al.*, Trapping of PARP1 and PARP2 by clinical PARP inhibitors. *Cancer Res.* **72**, 5588–5599 (2012).
9. Y. Pommier, M. J. O'Connor, J. de Bono, Laying a trap to kill cancer cells: PARP inhibitors and their mechanisms of action. *Sci. Transl. Med.* **8**, 362ps17 (2016).
10. T. A. Hopkins *et al.*, Mechanistic dissection of PARP1 trapping and the impact on in vivo tolerability and efficacy of PARP inhibitors. *Mol. Cancer Res.* **13**, 1465–1477 (2015).

11. Y. Pommier, Drugging topoisomerases: Lessons and challenges. *ACS Chem. Biol.* **8**, 82–95 (2013).
12. J. L. Delgado, C. M. Hsieh, N. L. Chan, H. Hiasa, Topoisomerases as anticancer targets. *Biochem. J.* **475**, 373–398 (2018).
13. M. D. Megonigal, J. Fertala, M. A. Bjornsti, Alterations in the catalytic activity of yeast DNA topoisomerase I result in cell cycle arrest and cell death. *J. Biol. Chem.* **272**, 12801–12808 (1997).
14. R. J. Reid *et al*., Selective ploidy ablation, a high-throughput plasmid transfer protocol, identifies new genes affecting topoisomerase I-induced DNA damage. *Genome Res.* **21**, 477–486 (2011).
15. L. Balakrishnan, R. A. Bambara, Flap endonuclease 1. *Annu. Rev. Biochem.* **82**, 119–138 (2013).
16. F. M. Pisani, E. Napolitano, L. M. R. Napolitano, S. Onesti, Molecular and cellular functions of the warsaw breakage syndrome DNA helicase DDX11. *Genes (Basel)* **9**, E564 (2018).
17. C. Bhattacharya, X. Wang, D. Becker, The DEAD/DEAH box helicase, DDX11, is essential for the survival of advanced melanomas. *Mol. Cancer* **11**, 82 (2012).
18. D. M. van Pel *et al*., An evolutionarily conserved synthetic lethal interaction network identifies FEN1 as a broad-spectrum target for anticancer therapeutic development. *PLoS Genet.* **9**, e1003254 (2013).
19. K. J. McManus, I. J. Barrett, Y. Nouhi, P. Hieter, Specific synthetic lethal killing of RAD54B-deficient human colorectal cancer cells by FEN1 silencing. *Proc. Natl. Acad. Sci. U.S.A.* **106**, 3276–3281 (2009).
20. J. L. McLellan *et al*., Synthetic lethality of cohesins with PARPs and replication fork mediators. *PLoS Genet.* **8**, e1002574 (2012).
21. V. K. Hill, J. S. Kim, T. Waldman, Cohesin mutations in human cancer. *Biochim. Biophys. Acta* **1866**, 1–11 (2016).
22. A. Losada, Cohesin in cancer: Chromosome segregation and beyond. *Nat. Rev. Cancer* **14**, 389–393 (2014).
23. A. Cornish-Bowden, The origins of enzyme kinetics. *FEBS Lett.* **587**, 2725–2730 (2013).
24. B. Shen, J. P. Nolan, L. A. Sklar, M. S. Park, Essential amino acids for substrate binding and catalysis of human flap endonuclease 1. *J. Biol. Chem.* **271**, 9173–9176 (1996).
25. B. Shen, J. P. Nolan, L. A. Sklar, M. S. Park, Functional analysis of point mutations in human flap endonuclease-1 active site. *Nucleic Acids Res.* **25**, 3332–3338 (1997).
26. R. Gary *et al*., A novel role in DNA metabolism for the binding of Fen1/Rad27 to PCNA and implications for genetic risk. *Mol. Cell. Biol.* **19**, 5373–5382 (1999).
27. A. L. Greene, J. R. Snipe, D. A. Gordenin, M. A. Resnick, Functional analysis of human FEN1 in Saccharomyces cerevisiae and its role in genome stability. *Hum. Mol. Genet.* **8**, 2263–2273 (1999).
28. C. Spiro, C. T. McMurray, Nuclease-deficient FEN-1 blocks Rad51/BRCA1-mediated repair and causes trinucleotide repeat instability. *Mol. Cell. Biol.* **23**, 6063–6074 (2003).
29. A. Hamza, M. R. M. Driessen, E. Tammpere, N. J. O'Neil, P. Hieter, Cross-species complementation of nonessential yeast genes establishes platforms for testing inhibitors of human proteins. *Genetics* **214**, 735–747 (2020).
30. X. Wu *et al*., Processing of branched DNA intermediates by a complex of human FEN-1 and PCNA. *Nucleic Acids Res.* **24**, 2036–2043 (1996).
31. J. Qiu *et al*., Interaction interface of human flap endonuclease-1 with its DNA substrates. *J. Biol. Chem.* **279**, 24394–24402 (2004).
32. A. Dudás, M. Chovanec, DNA double-strand break repair by homologous recombination. *Mutat. Res.* **566**, 131–167 (2004).
33. J. Qiu, D. N. Bimston, A. Partikian, B. Shen, Arginine residues 47 and 70 of human flap endonuclease-1 are involved in DNA substrate interactions and cleavage site determination. *J. Biol. Chem.* **277**, 24659–24666 (2002).
34. A. Hamza *et al*., Complementation of yeast genes with human genes as an experimental platform for functional testing of human genetic variants. *Genetics* **201**, 1263–1274 (2015).
35. A. Farina *et al*., Studies with the human cohesin establishment factor, ChlR1. Association of ChlR1 with Ctf18-RFC and Fen1. *J. Biol. Chem.* **283**, 20925–20936 (2008).
36. S. Rudra, R. V. Skibbens, Sister chromatid cohesion establishment occurs in concert with lagging strand synthesis. *Cell Cycle* **11**, 2114–2121 (2012).
37. C. P. Samora *et al*., Ctf4 links DNA replication with sister chromatid cohesion establishment by recruiting the Chl1 helicase to the replisome. *Mol. Cell* **63**, 371–384 (2016).
38. Y. Hirota, J. M. Lahti, Characterization of the enzymatic activity of hChlR1, a novel human DNA helicase. *Nucleic Acids Res.* **28**, 917–924 (2000).
39. Y. Wu, J. A. Sommers, I. Khan, J. P. de Winter, R. M. Brosh Jr., Biochemical characterization of Warsaw breakage syndrome helicase. *J. Biol. Chem.* **287**, 1007–1021 (2012).
40. S. L Holloway, CHL1 is a nuclear protein with an essential ATP binding site that exhibits a size-dependent effect on chromosome segregation. *Nucleic Acids Res.* **28**, 3056–3064 (2000).
41. G. O. Bylund, P. M. Burgers, Replication protein A-directed unloading of PCNA by the Ctf18 cohesion establishment complex. *Mol. Cell. Biol.* **25**, 5445–5455 (2005).
42. M. L. Mayer, S. P. Gygi, R. Aebersold, P. Hieter, Identification of RFC(Ctf18p, Ctf8p, Dcc1p): An alternative RFC complex required for sister chromatid cohesion in S. cerevisiae. *Mol. Cell* **7**, 959–970 (2001).
43. H. Ding, M. Guo, V. Vidhyasagar, T. Talwar, Y. Wu, The Q motif is involved in DNA binding but not ATP binding in ChlR1 helicase. *PLoS One* **10**, e0140755 (2015).
44. S. L. Gerring, F. Spencer, P. Hieter, The CHL 1 (CTF 1) gene product of Saccharomyces cerevisiae is important for chromosome transmission and normal cell cycle progression in G2/M. *EMBO J.* **9**, 4347–4358 (1990).
45. M. L. Mayer *et al*., Identification of protein complexes required for efficient sister chromatid cohesion. *Mol. Biol. Cell* **15**, 1736–1745 (2004).
46. R. V. Skibbens, Chl1p, a DNA helicase-like protein in budding yeast, functions in sister-chromatid cohesion. *Genetics* **166**, 33–42 (2004).
47. J. Fernius, K. G. Hardwick, Bub1 kinase targets Sgo1 to ensure efficient chromosome biorientation in budding yeast mitosis. *PLoS Genet.* **3**, e213 (2007).
48. K. W. Yuen *et al*., Systematic genome instability screens in yeast and their potential relevance to cancer. *Proc. Natl. Acad. Sci. U.S.A.* **104**, 3925–3930 (2007).
49. N. J. O'Neil, D. M. van Pel, P. Hieter, Synthetic lethality and cancer: Cohesin and PARP at the replication fork. *Trends Genet.* **29**, 290–297 (2013).
50. F. Uhlmann, SMC complexes: From DNA to chromosomes. *Nat. Rev. Mol. Cell Biol.* **17**, 399–412 (2016).
51. T. G. A. Reuvers, R. Kanaar, J. Nonnekens, DNA damage-inducing anticancer therapies: From global to precision damage. *Cancers (Basel)* **12**, E2098 (2020).
52. M. Petronczki *et al*., Sister-chromatid cohesion mediated by the alternative RF-CCtf18/Dcc1/Ctf8, the helicase Chl1 and the polymerase-alpha-associated protein Ctf4 is essential for chromatid disjunction during meiosis II. *J. Cell Sci.* **117**, 3547–3559 (2004).
53. S. Rudra, R. V. Skibbens, Chl1 DNA helicase regulates Scc2 deposition specifically during DNA-replication in Saccharomyces cerevisiae. *PLoS One* **8**, e75435 (2013).
54. Y. Wu, R. M. Brosh Jr., Helicase-inactivating mutations as a basis for dominant negative phenotypes. *Cell Cycle* **9**, 4080–4090 (2010).
55. L. Shen, J. Pelletier, Selective targeting of the DEAD-box RNA helicase eukaryotic initiation factor (eIF) 4A by natural products. *Nat. Prod. Rep.* **37**, 609–616 (2020).
56. D. M. Fowler, S. Fields, Deep mutational scanning: A new style of protein science. *Nat. Methods* **11**, 801–807 (2014).
57. D. M. Wilson III *et al*., Fragment- and structure-based drug discovery for developing therapeutic agents targeting the DNA damage response. *Prog. Biophys. Mol. Biol.* 10.1016/j.pbiomolbio.2020.10.005 (2020).
58. L. Zandarashvili *et al*., Structural basis for allosteric PARP-1 retention on DNA breaks. *Science* **368**, eaax6367 (2020).
59. L. N. Tumey *et al*., The identification and optimization of a N-hydroxy urea series of flap endonuclease 1 inhibitors. *Bioorg. Med. Chem. Lett.* **15**, 277–281 (2005).
60. J. C. Exell *et al*., Cellularly active N-hydroxyurea FEN1 inhibitors block substrate entry to the active site. *Nat. Chem. Biol.* **12**, 815–821 (2016).
61. T. A. Ward, P. J. McHugh, S. T. Durant, Small molecule inhibitors uncover synthetic genetic interactions of human flap endonuclease 1 (FEN1) with DNA damage response genes. *PLoS One* **12**, e0179278 (2017).
62. L. He *et al*., Targeting DNA flap endonuclease 1 to impede breast cancer progression. *EBioMedicine* **14**, 32–43 (2016).
63. S. E. Tsutakawa *et al*., Human flap endonuclease structures, DNA double-base flipping, and a unified understanding of the FEN1 superfamily. *Cell* **145**, 198–211 (2011).
64. S. E. Tsutakawa *et al*., Phosphate steering by Flap Endonuclease 1 promotes 5′-flap specificity and incision to prevent genome instability. *Nat. Commun.* **8**, 15855 (2017).
65. X. Yang *et al*., A public genome-scale lentiviral expression library of human ORFs. *Nat. Methods* **8**, 659–661 (2011).
66. Y. Hu *et al*., Approaching a complete repository of sequence-verified protein-encoding clones for Saccharomyces cerevisiae. *Genome Res.* **17**, 536–543 (2007).
67. S. Alberti, A. D. Gitler, S. Lindquist, A suite of Gateway cloning vectors for high-throughput genetic analysis in Saccharomyces cerevisiae. *Yeast* **24**, 913–919 (2007).
68. A. H. Kachroo *et al*., Evolution. Systematic humanization of yeast genes reveals conserved functions and genetic modularity. *Science* **348**, 921–925 (2015).
69. R. S. Sikorski, P. Hieter, A system of shuttle vectors and yeast host strains designed for efficient manipulation of DNA in Saccharomyces cerevisiae. *Genetics* **122**, 19–27 (1989).
70. G. Giaever *et al*., Functional profiling of the Saccharomyces cerevisiae genome. *Nature* **418**, 387–391 (2002).
71. T. W. Christianson, R. S. Sikorski, M. Dante, J. H. Shero, P. Hieter, Multifunctional yeast high-copy-number shuttle vectors. *Gene* **110**, 119–122 (1992).
72. W. K. Huh *et al*., Global analysis of protein localization in budding yeast. *Nature* **425**, 686–691 (2003).
73. Z. X. Xie *et al*., Rapid and efficient CRISPR/Cas9-Based mating-type switching of *Saccharomyces cerevisiae*. *G3 (Bethesda)* **8**, 173–183 (2018).
74. A. H. Tong *et al*., Systematic genetic analysis with ordered arrays of yeast deletion mutants. *Science* **294**, 2364–2368 (2001).
75. B. P. Young, C. J. Loewen, Balony: A software package for analysis of data generated by synthetic genetic array experiments. *BMC Bioinformatics* **14**, 354 (2013).
76. S. Duffy *et al*., Overexpression screens identify conserved dosage chromosome instability genes in yeast and human cancer. *Proc. Natl. Acad. Sci. U.S.A.* **113**, 9967–9976 (2016).
77. A. Hamza, K. Baetz, Iron-responsive transcription factor Aft1 interacts with kinetochore protein Iml3 and promotes pericentromeric cohesin. *J. Biol. Chem.* **287**, 4139–4147 (2012).